

Sub-micron silicon nitride waveguide fabrication using conventional optical lithography

Yuewang Huang, Qiancheng Zhao, Lobna Kamyab, Ali Rostami, Filippo Capolino & Ozdal Boyraz

EECS Department, University of California, Irvine, CA 92697, USA

oboyraz@uci.edu

Abstract: We demonstrate fabrication of sub- μm SiN waveguides using contact lithography with MEMS-grade photomasks for nonlinear optics and sensing applications that can provide 0.8dB/cm propagation loss, $\gamma=0.3\text{W}^{-1}/\text{m}$ nonlinearity, and $<100\text{ps}/\text{nm}\cdot\text{km}$ dispersion.

OCIS codes: 130.2790 Guided waves, 220.3740 Lithography, 230.7370 Waveguides.

1. Introduction

Recently, silicon nitride (SiN) has emerged as an alternative to silicon on insulator (SOI) platform for integrated photonic circuits [1–3]. Compared to silicon waveguides fabricated on expensive SOI wafers, the guiding layer made of SiN can be easily deposited in standard CMOS lines using plasma-enhanced vapor deposition (PECVD) or low pressure vapor deposition (LPCVD) on silicon wafers at very low cost. Unlike silicon, low propagation losses at both visible and near infrared are achievable in both PECVD and LPCVD deposited SiN waveguides [4,5]. These waveguides were generally fabricated by using E-beam lithography and stepper. It would be very attractive if the highly accessible UV contact lithography can be accommodated to fabricate low loss waveguides. However, the resolution limit of direct contact lithography is larger than $1\mu\text{m}$ due to optical diffraction limit. Even for large waveguides with dimension greater than $1\mu\text{m}$, high quality photomasks with smooth edges are still necessary in order to deliver low loss waveguides. In this report, we present such a fabrication technique that enables fabrication of sub-micron SiN waveguides using i-line UV contact lithography with very low cost MEMS grade photomasks. We show that a sequence of photolithography steps followed by KOH wet etching, thermal oxidation, and LPCVD SiN deposition can produce sub-micron trench like low loss waveguides that is suitable for microfluidic sensing and nonlinear optical applications. The process is also CMOS compatible. With this technique, we successfully fabricated SiN waveguide with a width of $0.8\mu\text{m}$ and effective mode area of $A_{\text{eff}}=1.9\mu\text{m}^2$. We achieved a low propagation loss of $0.8\pm 0.26\text{dB}/\text{cm}$. We also measured the nonlinear refractive index, effective nonlinearity and group velocity dispersion as $n_2=1.39\times 10^{-19}\text{m}^2/\text{W}$, $\gamma=0.3\text{W}^{-1}/\text{m}$, and $D<100\text{ps}/\text{nm}\cdot\text{km}$, respectively.

2. Fabrication of waveguides: line reduction and roughness smoothing

In order to fabricate sub-micron waveguide by using conventional optical lithography, there are two major challenges. First, the resolution of contact lithography is $>1\mu\text{m}$ and special photo resist and high quality masks have to be used in order to get close to this limit or go below this limit. Also, MEMS grade masks often have a large critical dimension and it is impossible to fabricate sub-micron waveguide by direct patterning. Hence a linewidth reduction mechanism has to be established. Second, due to limited resolution, features on photomasks tend to have rough edges as shown in Figure 1(a). This would lead to formidable scattering loss when used to directly pattern optical waveguide. Special methods have to be adopted to smoothen the edge roughness. In our fabrication, these two mechanisms are achieved by utilizing the anisotropic KOH etching and thermal oxidation. The fabrication process is shown in Figure 1b. A layer of 500nm SiO_2 and $1.2\mu\text{m}$ PR are first deposited and coated on the substrate. The PR layer is patterned with contact UV photo-lithography by using a low-cost MEMS grade photomask consisting of straight line openings with a critical dimension (CD) of $4\mu\text{m}$. The PR is developed later on to form large line openings of W_{top} to feature the photomask pattern after UV exposure at 365nm . Afterwards, the pattern is transferred to the oxide layer by ICP etching to form a hard mask for the following KOH etching. KOH etches the silicon substrate along the $\langle 100 \rangle$ direction for a depth of H_{Si} . Since the KOH silicon etching is highly anisotropic and etching rate along $\langle 111 \rangle$ direction is extremely slow, the wet etching will essentially stop at the (111) plane and trapezoidal or triangular shape trenches will be formed as shown in the 6th diagram in Figure 1(b). The slope follows the (111) plane and forms an angle of $\tan^{-1}\sqrt{2} = 54.7^\circ$. As a result, V-grooves will be etched if the linewidth (W_{top}) on the photomask is smaller than $2 \times \frac{\sqrt{2}}{2} \times H_{\text{Si}}$. On the other hand, if the original linewidth is larger than that amount,

the KOH etching will create an inverted isosceles trapezoidal shape with the lower edge $2 \times \frac{\sqrt{2}}{2} \times H_{Si}$ smaller than the upper edge, which equals the linewidth on the photomask. For example, if the linewidth of the openings on the photomask is $5\mu\text{m}$, the lower edge of the etched trenches will be only $W_{\text{btm}} = 5 - 2 \times \frac{\sqrt{2}}{2} \times 3 = 0.8\mu\text{m}$ given a Si etching depth of $3\mu\text{m}$. Sub-micron linewidth is achieved by using this line reduction technique based on KOH etching. KOH wet etching also smoothes the line edges. Figure 1(d) shows the effect of roughness smoothing in the KOH etching. The line edges after the KOH etching in Figure 1(d) are dramatically smoothed compared to the patterns on the (b) photomask and (c) PR layer. After removing oxide hard mask, a layer of $3\mu\text{m}$ thermal oxide is grown to serve as a buffer layer to isolate the optical field from leaking into the silicon substrate. Thermal oxidation also helps on roughness smoothing. Hereafter, a nitride layer of 725nm was deposited on the sample and in the oxidized trenches using LPCVD. The optical wave will be guided in the nitride in the valley of the trenches and such feature is attractive for introducing microfluidics into the same platform.

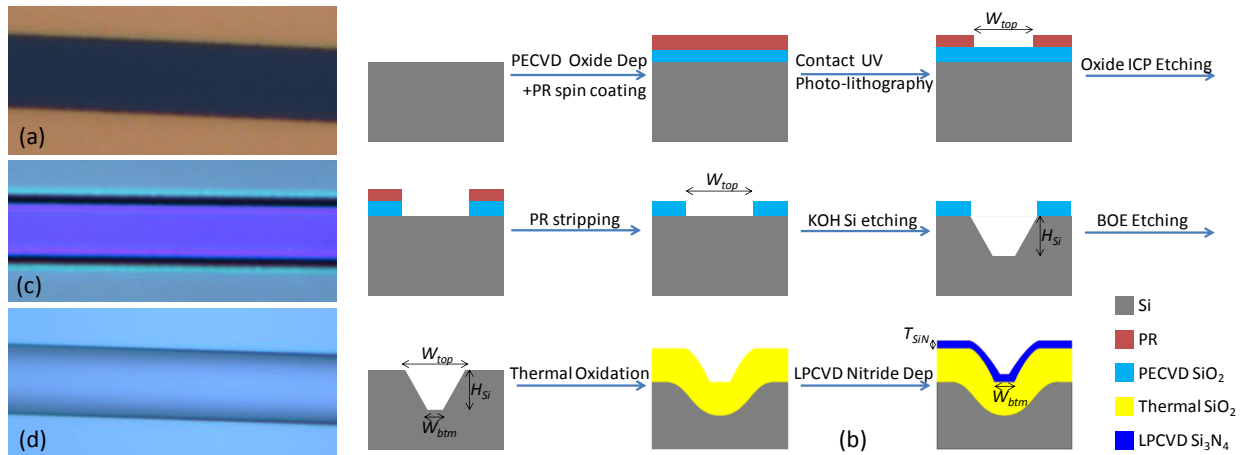


Figure 1. Fabrication process flow. A final annealing step is not shown in the figure. Roughness smoothing by KOH wet etching. (b) Optical microscope graph of the photomask with $5\mu\text{m}$ linewidth: edge roughness is observable; (c) optical microscope graph of the PR pattern: the edge roughness is transferred to the PR pattern; (d) Optical microscope graph of the pattern after KOH etching: the edges are dramatically smoothed.

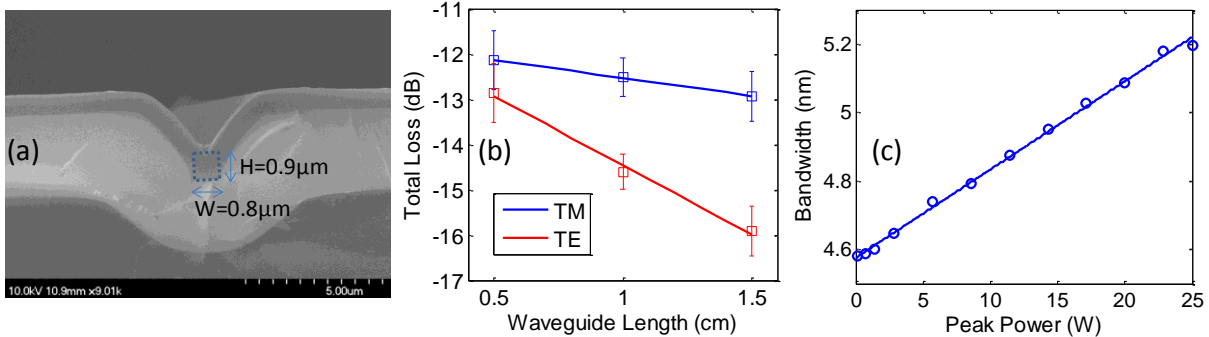


Figure 2. (a) SEM of the fabricated waveguide. (b) Total loss of waveguide with different length using cut-back method. (c) SPM broadening at different input peak power levels. A nonlinear refractive index of $n_2=1.39 \times 10^{-19} \text{m}^2/\text{W}$ was derived from the curve.

3. Waveguide Experimental Characterization

Figure 2(a) shows the SEM images of the fabricated waveguide with starting width of $W_{\text{top}}=5\mu\text{m}$. The dimension of the waveguide is $W_{\text{btm}} \times H_{\text{SiN}} = \sim 0.8\mu\text{m} \times 0.9\mu\text{m}$. After the waveguide fabrication, we diced the waveguides and polished the waveguide ends with lapping films for optical quality facets. We then characterized the waveguide loss using the cut-back method. As shown in Figure 2(b), we measure the total loss of the waveguides with three different lengths: $L=0.5\text{cm}$, 1cm and 1.5cm respectively. We derived a waveguide propagation loss of $0.8 \pm 0.26 \text{dB/cm}$ for TM mode. As expected, the fabricated waveguides are polarization sensitive and TE mode has higher propagation loss of $3.13 \pm 0.37 \text{dB/cm}$ due to leakage to the top nitride slab. The waveguide loss can be further reduced by using stoichiometric nitride or increasing the KOH etching depth H_{Si} . To possibly facilitate nonlinear

applications in these waveguides, we also characterized the nonlinear property of the waveguides, particularly the nonlinear refractive index, n_2 , of the silicon nitride. Here, we measured the nonlinear refractive index by utilizing the spectral broadening caused by self-phase-modulation (SPM) of high energy pulses in nonlinear medium [6,7]. Figure 2(c) shows the 3dB bandwidth of the fs laser pulse at waveguide output with different input peak power. With the propagation loss of 0.8dB/cm from loss measurement and an effective mode area of $A_{\text{eff}}=1.9\mu\text{m}^2$, we estimated a nonlinear refractive index value of $n_2=1.39\times 10^{-19}\text{m}^2/\text{W}$ from the slope of the fitted linear curve. This value agrees well with the values reported in other literatures [4,7]. We also calculated a nonlinear parameter of $\gamma = \frac{\omega n_2}{c A_{\text{eff}}} = 0.3\text{W}^{-1}/\text{m}$ for the waveguide, which is >100 times larger than that in single-mode fibers.

4. Waveguide Numerical Characterization

We also put these structures defined by SEM images into COMSOL to further investigate the properties of the waveguides. The refractive index of the SiN film was measured using ellipsometry. Figure 3(a) and (b) shows the simulated mode profile of the fundamental TM and TE mode of the waveguides. The mode profiles are of heart shape. The TM mode is more concentrated in the SiN than TE mode, which leads to a higher effective index in the TM mode as shown in Figure 3(c). This also agrees with the propagation loss measurements in the previous section. However, the effective mode area of TM mode is large than TE mode as shown in Figure 3(d). The effective mode area is $\sim 1.9\mu\text{m}^2$ and $\sim 1.55\mu\text{m}^2$ for TM and TE mode. This type of waveguide can also be designed to have strong evanescent field in the trenches for enhanced interaction with micro fluid or plasmonic coating in sensing applications. Figure 3(e) shows the calculated dispersion of the silicon nitride waveguide. Both the TM and TE mode are in the anomalous dispersion region and very small dispersion values are expected in these waveguides in the telecommunication window, which makes them very promising for nonlinear parametric process requiring phase matching, e.g. four-wave-mixing (FWM) applications. The TM mode shows lower dispersion than TE mode.

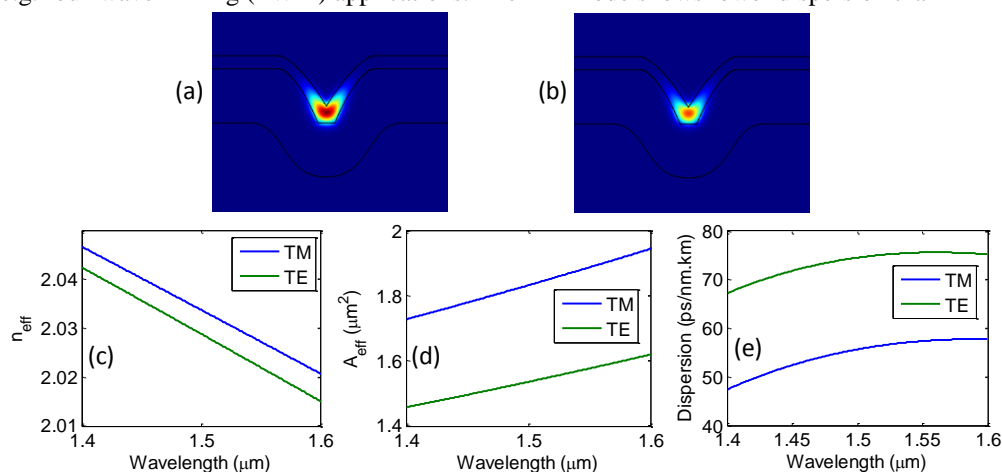


Figure 3. Numerical simulation results for the waveguide: (a) TM mode profile; (b) TE mode profile; (c) effective mode index; (d) effective mode area; (e) GVD dispersion.

This research was partially supported by the National Science Foundation (NSF) Award No. ECCS-1028727.

1. D. D. John, M. J. R. Heck, J. F. Bauters, R. Moreira, J. S. Barton, J. E. Bowers, and D. J. Blumenthal, "Multilayer Platform for Ultra-Low-Loss Waveguide Applications," *IEEE Photonics Technol. Lett.* **24**, 876–878 (2012).
2. D. J. Moss, R. Morandotti, A. L. Gaeta, and M. Lipson, "New CMOS-compatible platforms based on silicon nitride and Hydex for nonlinear optics," *Nat. Photonics* **7**, 597–607 (2013).
3. S. Romero-García, F. Merget, F. Zhong, H. Finkelstein, and J. Witzens, "Silicon nitride CMOS-compatible platform for integrated photonics applications at visible wavelengths," *Opt. Express* **21**, 14036–14046 (2013).
4. K. Ikeda, R. E. Saperstein, A. Alic, and Y. Fainman, "Thermal and Kerr nonlinear properties of plasma-deposited silicon nitride/ silicon dioxide waveguides," *Opt. Express* **16**, 12987–12994 (2008).
5. S. Minissale, S. Yerci, and L. D. Negro, "Nonlinear optical properties of low temperature annealed silicon-rich oxide and silicon-rich nitride materials for silicon photonics," *Appl. Phys. Lett.* **100**, 021109 (2012).
6. C.-Y. Tai, J. S. Wilkinson, N. M. Perney, M. C. Netti, and J. J. Baumberg, "Self-phase modulation induced spectral broadening of ultrashort laser pulses in tantalum pentoxide (Ta) rib waveguide," (2003).
7. J. Levy, "Integrated Nonlinear Optics In Silicon Nitride Waveguides And Resonators," (2011).